Supplementary information files for Temperature control of diffusive memristor hysteresis and artificial neuron spiking

Temperature control of diffusive memristor hysteresis and artificial neuron spiking

D.P. Pattnaik, Y. Ushakov, Z. Zhou, P. Borisov, M.D. Cropper, U.W. Wijayantha, A.G. Balanov and S.E. Savelev

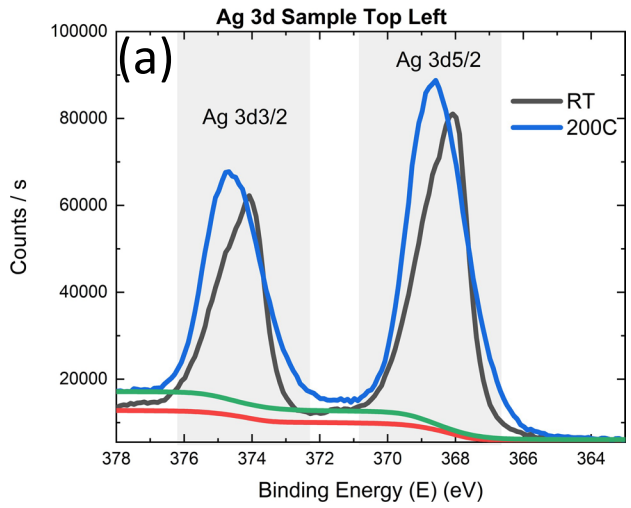

(a)

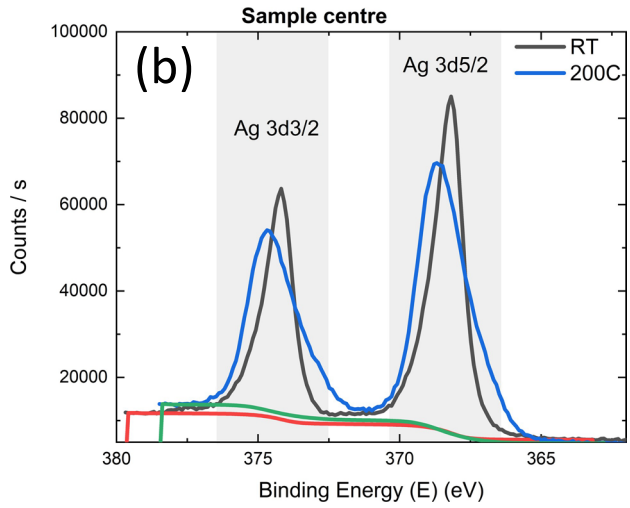

(b)

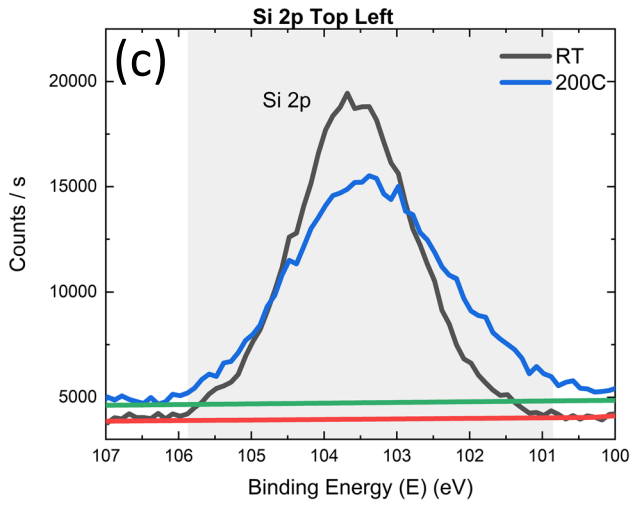

(c)

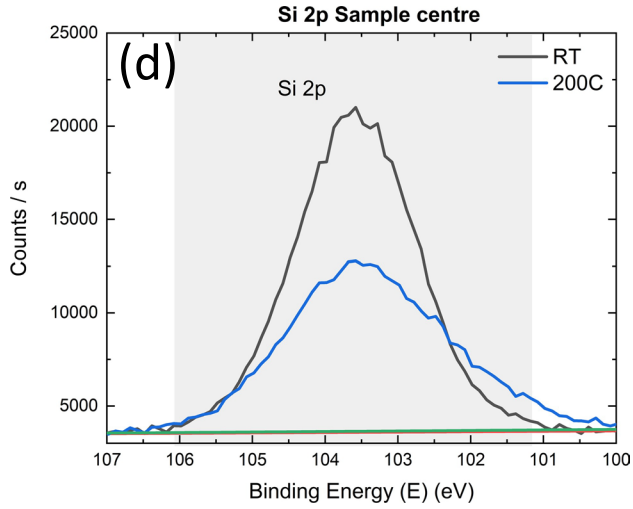

(d)

Supplementary Figure S1. X-ray Photoelectron Spectroscopy (XPS) of a SiOx:Ag diffusive memristor sample at different position across the sample surface. The intensity of the Ag 3d and Si 2p are shown for the sample at RT (black), and after a heat treatment at 200 C (Blue). There is a shift by 0.5eV in the Ag binding energy which would correlate to different sizes of the Ag nanoparticles pre and post heat treatment [20], as evident from the TEM images shown in Fig. 2 (d).

Silver Percentage (At%)	Sample A As-grown sample	Sample B 200°C
Top Left	12.24	12.77
Top Right	10.36	14.22
Mid	7.55	12.13
Bottom Left	9.24	12.19
Bottom Right	12.89	13.76

Supplementary Table T1. Table showing the Ag atomic concentration at different sites of our sample (10x10mm in dimension). Sample A is an as-grown sample, and Sample B is for the sample subjected to heating upto 200 C. There is a net increase in the Ag concentration across the locations of the sample.

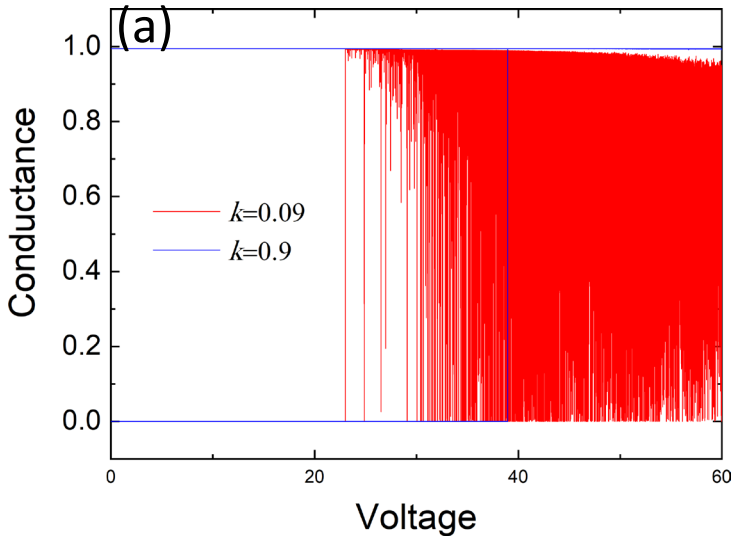

(a)

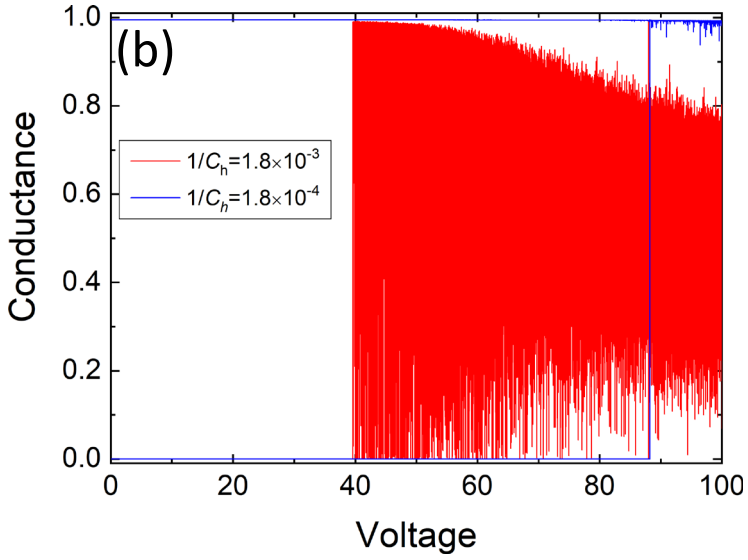

(b)

Supplementary Figure S2: Resetting the memristor state in our diffusive memristor can also be achieved by decreasing the (a) the heat transfer coefficient k and (b) specific heat capacity C_h of a diffusive memristor. Here, the model predicts that by decreasing the heat transfer coefficient k or the specific heat capacity C_h of our device, it is possible to reset the permanent LRS instead of changing the device temperature which has irreversible effects and can damage the sample.

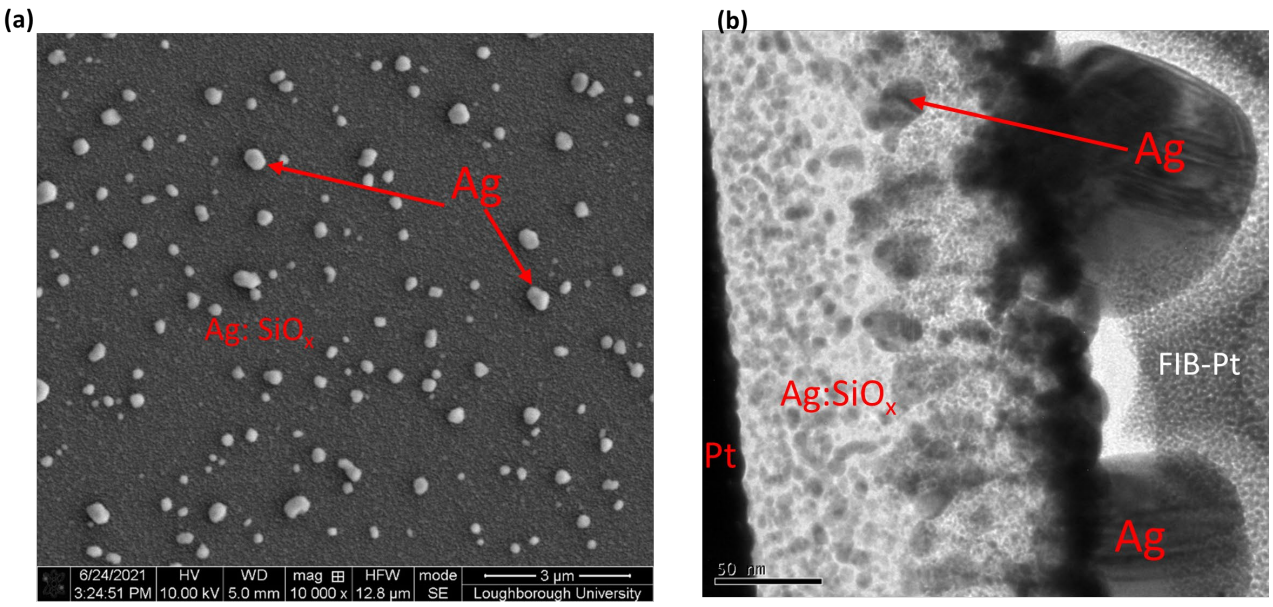

Supplementary Figure S3: (a) SEM and (b) TEM images of Ag nanoclusters in our diffusive memristors samples after a heat treatment at 200 C. Larger Ag clusters appear on the sample surface and can be clearly observed. This is due to sintering of Ag and is due to Ostwald ripening [43,44]

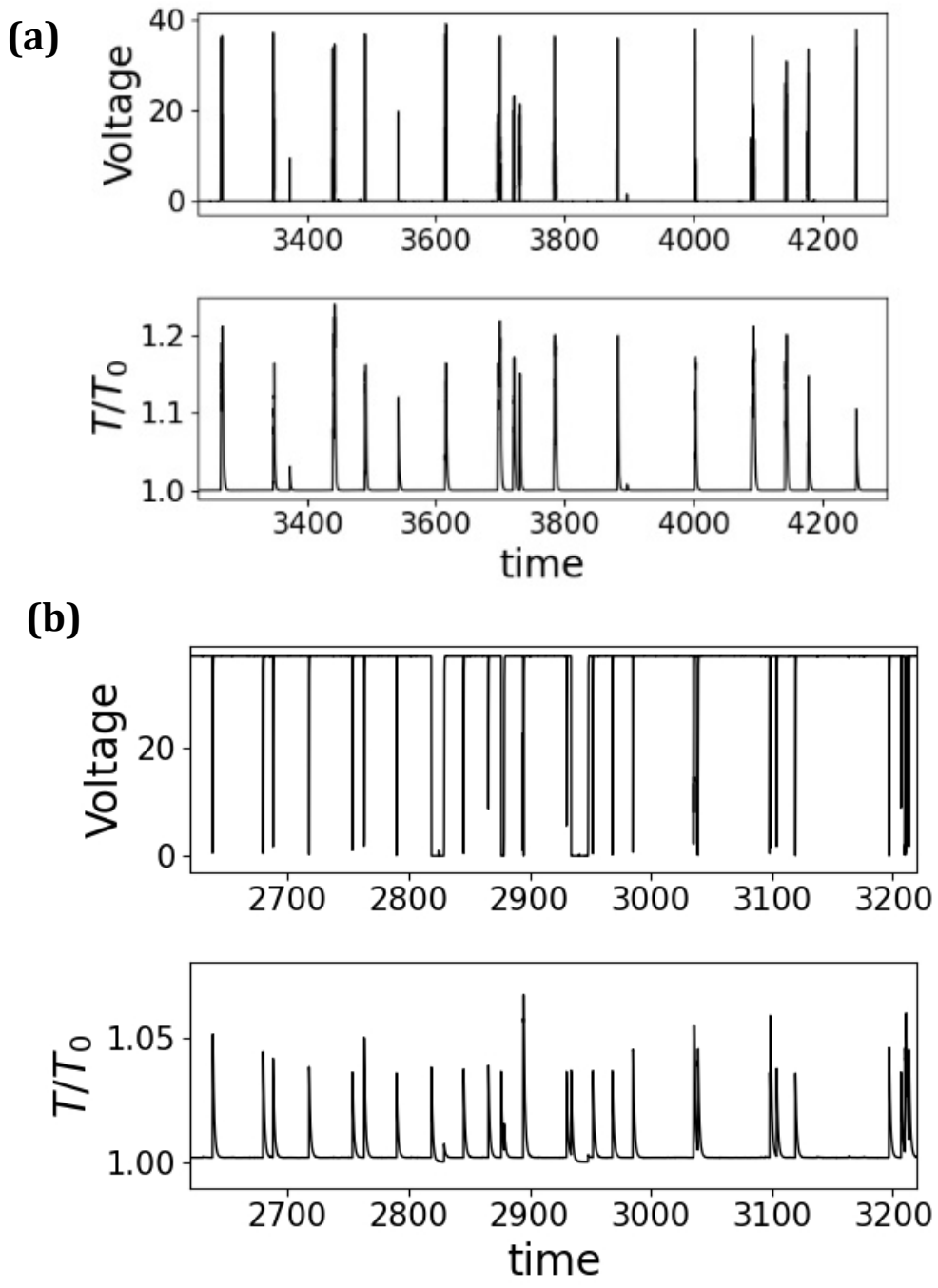

Supplementary Figure S4: Estimated temperature variation during switching of our memristor device during transition from (a) HRS to LRS and (b) LRS to HRS

SIMULATION DETAILS

A. Obtaining dimensionless system of equations

The full original system of equations is

$$\begin{cases} \eta\dfrac{dx}{dt} = -\dfrac{\partial U(x)}{\partial x} + q\dfrac{V}{L} + \sqrt{2k_B\eta T}\xi(t) \\ \dfrac{dT}{dt} = \dfrac{V^2}{C_h R(x)} - k(T - T_0) \\ \tau\dfrac{dV}{dt} = V_{ext} - \left(1 + \dfrac{R_{ext}}{R(x)}\right)V, \end{cases} \tag{1}$$

where $R(x) = R_0\cosh(x/\lambda)$, and all the parameters and variables are explained in the paper text.

Let us substitute the following expressions

$$\begin{gathered} x = L\tilde{x}, t = t_N\tilde{t}, V = V_N\tilde{V}, q = q_0/2, \\ U(x) = \Delta U\tilde{U}(\tilde{x}), k_BT = T_N\tilde{T}, C_h = C_N\tilde{C}_h, \\ k = k_N\tilde{k}, V_{ext} = V_N\tilde{V}_{ext}, R(x) = R_0\tilde{R}(\tilde{x}), \\ R_{ext} = R_0\tilde{R}_{ext}, \tau = t_N\tilde{\tau}, \xi(t) = \tilde{\xi}(\tilde{t})/\sqrt{t_N} \end{gathered} \tag{2}$$

where $\tilde{x}$ is the dimensionless version of x and the same for the other variables.

$$\begin{cases} \dfrac{\eta L}{t_N}\dfrac{d\tilde{x}}{d\tilde{t}} = -\dfrac{\Delta U}{L}\dfrac{\partial\tilde{U}(\tilde{x})}{\partial\tilde{x}} + \dfrac{q_0V_N}{L}\dfrac{\tilde{V}}{2} + \sqrt{2\eta T_N}\dfrac{\sqrt{\tilde{T}}}{\sqrt{\tilde{t}_N}}\tilde{\xi}(\tilde{t}) \\ \dfrac{T_N}{t_N}\dfrac{d\tilde{T}}{d\tilde{t}} = \dfrac{k_BV_N^2}{C_NR_0}\dfrac{\tilde{V}^2}{\tilde{C}_h\tilde{R}(\tilde{x})} - k_NT_N\tilde{k}(\tilde{T} - \tilde{T}_0) \\ \tilde{\tau}\dfrac{d\tilde{V}}{d\tilde{t}} = \tilde{V}_{ext} - \left(1 + \dfrac{\tilde{R}_{ext}}{\tilde{R}(\tilde{x})}\right)\tilde{V} \end{cases} \tag{3}$$

$$\begin{cases} \dfrac{d\tilde{x}}{d\tilde{t}} = -\dfrac{t_N\Delta U}{\eta L^2}\dfrac{\partial\tilde{U}(\tilde{x})}{\partial\tilde{x}} + \dfrac{q_0V_Nt_N}{\eta L^2}\dfrac{\tilde{V}}{2} \\ \qquad + \sqrt{\dfrac{2T_Nt_N}{\eta L^2}}\sqrt{\tilde{T}}\tilde{\xi}(\tilde{t}) \\ \dfrac{d\tilde{T}}{d\tilde{t}} = \dfrac{t_Nk_BV_N^2}{T_NC_NR_0}\dfrac{\tilde{V}^2}{\tilde{C}_h\tilde{R}(\tilde{x})} - k_Nt_N\tilde{k}(\tilde{T} - \tilde{T}_0) \\ \tilde{\tau}\dfrac{d\tilde{V}}{d\tilde{t}} = \tilde{V}_{ext} - \left(1 + \dfrac{\tilde{R}_{ext}}{\tilde{R}(\tilde{x})}\right)\tilde{V} \end{cases} \tag{4}$$

So, all the normalization constants can be expressed through the real physical characteristics:

$$\begin{gathered} t_N = \frac{\eta L^2}{\Delta U}, V_N = \frac{\Delta U}{q_0}, T_N = \frac{\Delta U}{2}, \\ C_N = \frac{t_Nk_BV_N^2}{T_NR_0}, k_N = \frac{1}{t_N}, \end{gathered} \tag{5}$$

therefore providing the dimensionless equations:

$$\begin{cases} \dfrac{d\tilde{x}}{d\tilde{t}} = -\dfrac{\partial\tilde{U}(\tilde{x})}{\partial\tilde{x}} + \tilde{V}/2 + \sqrt{\tilde{T}}\tilde{\xi}(\tilde{t}) \\ \dfrac{d\tilde{T}}{d\tilde{t}} = \dfrac{\tilde{V}^2}{\tilde{C}_h\tilde{R}(\tilde{x})} - \tilde{k}(\tilde{T} - \tilde{T}_0) \\ \tilde{\tau}\dfrac{d\tilde{V}}{d\tilde{t}} = \tilde{V}_{ext} - \left(1 + \dfrac{\tilde{R}_{ext}}{\tilde{R}(\tilde{x})}\right)\tilde{V} \end{cases} \tag{6}$$

Then, we rid the variables of tildes so that getting the equations presented in the paper.

B. Scaling

In Fig. 5 of the main article, the simulated curves have been scaled to fit the experimental data. That was not done sistematically throughout the whole paper as we only tried to demonstrate the qualitative match. Nevertheless, given the expressions (5) and the one for $R(x)$, one can see that V, T and the current $I = V/R(x)$ can be consistently scaled almost independently by adjusting $q_0, \Delta U$, and R_0. Given this kind of scaling one could establish some good quantitative correspondence between the theory and the experiment, but that would require special experimental data, which we were not focused on.

To put experimental and theoretical curves within the same axes in Figs. 5(a,b) we used the following conversions: $T_{exp} = 130 \cdot T_{theory} - 120, V_{exp} = 0.435 \cdot V_{theory}, I_{exp} = 2 \cdot 10^{-5} \cdot I_{theory}$. As one can see, theoretical temperature values have been shifted by a constant value, which is equivalent to $k_BT = T_N(\tilde{T} + \theta)$ conversion in (2) with an additional constant θ. This addition would change only the noise term in the first equation in (6) to $\sqrt{(\tilde{T} + \theta)}\tilde{\xi}(\tilde{t})$, but this does not influence the noise model in any way. The additional noise θ can be attributed to external electric noise, not directly related to thermal fluctuations.

C. Potential

To model the derivative of the temperature-dependent potential we used the following expression:

$$\begin{aligned} \frac{\partial U(x, T_0)}{\partial x} = \frac{1 + 0.1T_0^2}{(x+1)^2} - \frac{0.1}{(x+1)^3} \\ - \frac{2.5585(1 + 0.01T_0)}{(x - 0.845)^{44}} - \frac{2.2}{(x - 0.845)^{45}}. \end{aligned}$$

The temperature independent potential derivative was just the same but with $T_0 \equiv 0$.

D. Simulation parameters

The following (dimensionless) parameters were used for the simulations:

$$k = 0.9, \lambda = 0.065, C_h = 5000.$$

For the spiking artificial neuron we also used:

$$R_{ext} = 2000, \tau = 0.1, V_{ext} = 37.$$